IJCFD, 2000, Vol. 13, pp. 185–202
Reprints available directly from the publisher
Photocopying permitted by license only

Evolution of Concentrated Vortices in a Viscous Fluid

E. A. BABKIN[a], V. A. BRAILOVSKAYA[b], D. CLAMOND[c], PH. FRAUNIE[c] and YU. A. STEPANYANTS[a,b,*]

[a] *Department of Applied Mathematics, NNTU, Nizhny Novgorod, Russia;* [b] *Institute of Applied Physics, Russian Academy of Science, Nizhny Novgorod, Russia;* [c] *LSEET, Université de Toulon et du Var, La Garde, France*

(Received 5 August 1998; In final form 24 March 1999)

Evolution of the vortices of monopole and dipole types in a viscous fluid is considered numerically. Theory and numerical results are compared for some particular exact solutions. A good agreement is obtained for the dipole vortices (viscous Chaplygin-Lamb vortices) moving with variable velocities due to viscosity. For the monopole type vortices, the agreement is more or less good only at an initial stage of their evolution; while in the long-time asymptotics the law of vorticity decay other than the theoretical one is discovered. The reason for such a discrepancy is discussed. The interactions of dipole vortices with each other and with rigid boundaries are studied too. The stability of dipole vortices with complex internal structures is considered briefly.

Keywords: Viscous fluids, vortices, exact solutions, numerical study, Chaplygin-Lamb vortices, vortex interaction, vortex stability

1. INTRODUCTION

Dynamics of concentrated vortices in a viscous fluid is an interesting and important problem of modern hydrodynamics which has many applications to different physical and technical branches. It has been studied intensively by many researchers, but some important questions still remain unanswered. Only a few analytical solutions for vortices in a perfect fluid are known at the present. These include three-dimensional Hill's vortex and the two-dimensional Chaplygin-Lamb (ChL) vortex, Lamb (1932); Batchelor (1970); Meleshko and Van Heijst (1994). Until recently, only one exact solution was known for viscous fluid. This solution describes the evolution of an isolated single vortex of the monopole type, Kochin, Kibel' and Rose (1963); Batchelor (1970); Saffman (1992) and represents diffusion of vorticity from a singular initial state. One more exact solution was recently obtained for a pair of initially singular vortices with equal intensities that diffuse and rotate along a spiral trajectory in the course of evolution and decay, Agullo and Verga (1997). Numerous papers were devoted to approximate analytical and numerical solutions for vortex structures and vortex

*Corresponding author.

dynamics in a viscous fluid (see, *e.g.*, Berezovsky and Kaplansky (1992) and the cited literature).

One of the most intriguing objects for vortex application is hydrodynamic turbulence. The idea is to present developed turbulence as a chaotic ensemble of interacting nonlinear patterns similar to soliton gas in a fixed volume. Concentrated quasistationary vortices could be considered as the "elementary particles" representing these patterns. That is why their existence, structure and dynamics are topical until now.

In this paper we investigate numerically vortex dynamics of the monopole and dipole types in viscous incompressible fluids with two different kinds of viscosity: internal, or Reynolds viscosity caused by the friction of fluid particles with each other, and external, or Rayleigh viscosity caused by the friction of fluid at the bottom and/or at the wall of the basin. In addition, we consider the influence of fluid rotation (both uniform and nonuniform in a β-plane approximation) on the decay of vortices.

The basic model equation used here is the viscosity-modified two-dimensional Charny-Obukhov equation (or Hasegawa-Mima equation in the plasma physics context), Pedlosky (1987); Kamenkovich *et al.* (1988); Petviashvili and Pokhotelov (1992); Nezlin and Snezhkin (1993). Written for the stream function $\psi(x, y, t)$ it has a form

$$\frac{\partial}{\partial t}(\Delta\psi - a^2\psi) + \beta\frac{\partial\psi}{\partial x} + J(\psi, \Delta\psi) = \nu\Delta^2\psi - \gamma\Delta\psi, \qquad (1)$$

so that the velocity can be represented as $\mathbf{v} = (-\psi_y, \psi_x)$. The other parameters in the equation are the following: $a^{-2} \equiv \mathrm{Ro}^2 = gh/f^2$ is a square of the Rossby-Obukhov parameter (where Ro is a radius of deformation in geophysical fluid dynamics); g is acceleration due to gravity; h, unperturbed basin depth; f, Coriolis parameter (double local frequency of fluid rotation); β is a gradient of the Coriolis parameter along the meridian; $J(\psi,\varphi) \equiv \psi_x\varphi_y - \psi_y\varphi_x$ is a Jacobian of two functions; and Δ is a two-dimensional Laplace operator. All details can be found in the books cited above, Pedlosky (1987); Kamenkovich *et al.* (1988); Petviashvili and Pokhotelov (1992); Nezlin and Snezhkin (1993).

The first term in the right-hand side of (1) corresponds to conventional internal viscosity, while the second one describes fluid friction at the bottom of the basin and/or at the walls of a tank in laboratory experiments, Dolzhansky *et al.* (1990).

Some exact solutions of (1) are known in the absence of viscosity. These are dipole Stern and Larichev-Reznik (LR) vortices in the β-plane and in the f-plane (when $\beta = 0$, but $a \neq 0$), Stern (1975); Larichev and Reznik (1976); Flierl *et al.* (1980) and ChL vortices in a perfect nonrotating fluid ($\beta = a = 0$), Lamb (1932); Batchelor (1970); Meleshko and Van Heijst (1994). We also note that for $\beta = 0$ any stationarily rotating vortex of the monopole type is an exact solution of the inviscid Eq. (1) (*i.e.*, ψ can be an arbitrary function of radial coordinate $r = \sqrt{x^2 + y^2}$).

Here, we study numerically the influence of both types of viscosity upon monopole and dipole types of vortices. Our paper is organized as follows. Two different numerical schemes used in our computations are described in Section 2. Then, we present in Section 3 numerical results for dynamics of monopole vortices. In Section 4 we study the evolution of single dipole vortices in viscous fluid. The interactions of dipole vortices, as well as stability of dipole vortices with complex internal structures are studied in Section 5. Some general discussions and conclusions are presented in Section 6.

2. NUMERICAL SCHEMES

Our research was carried out using two different schemes for solution of Navier-Stokes equations and their generalization to rotating shallow water with external viscosity.

2.1. The First Method

The first method is used for a 2D plane domain with *fixed* boundary conditions. It corresponds to the demand $\mathbf{v} = 0$ at the walls. The corresponding

numerical scheme was elaborated for solution of Eq. (1) with zero parameters a and γ. In this case, Eq. (1) reduces to the following simple form:

$$\frac{\partial}{\partial t}\Delta\psi + J(\psi, \Delta\psi) = \nu\Delta^2\psi. \tag{2}$$

It is convenient to represent this equation in ω,ψ variables:

$$\frac{\partial\omega}{\partial t} + J(\psi,\omega) = \nu\Delta\omega, \tag{3}$$

$$\omega = \Delta\psi, \tag{4}$$

where ω is vorticity.

2.1.1. *Discretization*

The centered spatial difference for Eq. (3) is used with Crank-Nicolson time differentiation for the diffusion term $\Delta\omega$, and the second-order Adams-Bashforth time differentiation is used for the convective term $J(\psi,\omega)$. This scheme can be obtained from the Taylor expansion of arbitrary function $z(x, y, t)$:

$$z_{i,j}^{n+1} \approx z_{i,j}^{n} + \left(\frac{\partial z}{\partial t}\right)_{i,j}^{n}\delta t + \frac{1}{2}\left(\frac{\partial^2 z}{\partial t^2}\right)_{i,j}^{n}\delta t^2,$$

where index n corresponds to time steps, while indexes i and j correspond to spatial discretization on x and y.

The second-order derivative term can be approximated as:

$$\left(\frac{\partial^2 z}{\partial t^2}\right)_{i,j}^{n} = \frac{\partial}{\partial t}\left(\frac{\partial z}{\partial t}\right)_{i,j}^{n} \approx \frac{\left(\frac{\partial z}{\partial t}\right)_{i,j}^{n} - \left(\frac{\partial z}{\partial t}\right)_{i,j}^{n-1}}{\delta t}.$$

Finally, the difference scheme can be written in the form:

$$z_{i,j}^{n+1} \approx z_{i,j}^{n} + \frac{3}{2}\left(\frac{\partial z}{\partial t}\right)_{i,j}^{n}\delta t - \frac{1}{2}\left(\frac{\partial z}{\partial t}\right)_{i,j}^{n-1}\delta t.$$

Applying this formula to Eq. (3) we obtain:

$$\omega_{i,j}^{n+1} - \frac{\nu\delta t}{2}(\Delta\omega)_{i,j}^{n+1} = \omega_{i,j}^{n} + \frac{\nu\delta t}{2}(\Delta\omega)_{i,j}^{n} + \frac{\delta t}{2}\left[\frac{\partial}{\partial x}(u\omega) + \frac{\partial}{\partial y}(v\omega)\right]\Bigg|_{i,j}^{n-1} - \frac{3\delta t}{2}\left[\frac{\partial}{\partial y}(u\omega) + \frac{\partial}{\partial x}(v\omega)\right]\Bigg|_{i,j}^{n}. \tag{5}$$

Now the problem that must be solved at each time step can be written as:

$$\omega_{i,j}^{n+1} - \frac{\nu\delta t}{2}(\Delta\omega)_{i,j}^{n+1} = F(\omega_{i,j}^{n}, u_{i,j}^{n}, v_{i,j}^{n}, \omega_{i,j}^{n-1}, u_{i,j}^{n-1}, v_{i,j}^{n-1}),$$

where F is the discrete source term from the right-hand side of Eq. (5).

This elliptic partial differential equation can be solved by an iterative method at each time step. For this reason we introduce a fictitious time step τ and iterations over each time level for the following equation:

$$\frac{\partial\omega}{\partial\tau} + \omega - \frac{\nu\delta t}{2}\Delta\omega = F(\omega_{i,j}^{n}, u_{i,j}^{n}, v_{i,j}^{n}, \omega_{i,j}^{n-1}, u_{i,j}^{n-1}, v_{i,j}^{n-1}). \tag{6}$$

(Further we will notice time steps in the "real" time t with the index n, while in the fictious time τ with the index k.)

The alternative-directions implicit scheme was used to solve Eq. (6). Monotonic approximation of space derivatives in the source terms in the right-hand side of Eq. (5) was used with progressive compensation of artificial viscosity, Samarsky (1977). The corresponding set of equations on a non-uniform grid is written as:

$$h_x = h(i), \quad i = 1, 2, \ldots, N_x;$$
$$h_y = h(j), \quad j = 1, 2, \ldots, N_y;$$

For equal space steps h_x and h_y the above system can be written as follows:

$$\begin{cases} \dfrac{\omega_{i,j}^{k+\frac{1}{2}} - \omega_{i,j}^{k}}{\tau/2} + \omega_{i,j}^{k+\frac{1}{2}} \\ -\dfrac{\nu\delta t}{2}\left[\dfrac{2}{h_i + h_{i-1}}\left(\dfrac{\omega_{i+1,j}^{k+\frac{1}{2}} - \omega_{i,j}^{k+\frac{1}{2}}}{h_i} - \dfrac{\omega_{i,j}^{k+\frac{1}{2}} - \omega_{i-1,j}^{k+\frac{1}{2}}}{h_{i-1}}\right)\right. \\ \left. + \dfrac{2}{h_j + h_{j-1}}\left(\dfrac{\omega_{i,j+1}^{k} - \omega_{i,j}^{k}}{h_j} - \dfrac{\omega_{i,j}^{k} - \omega_{i,j-1}^{k}}{h_{j-1}}\right)\right] \\ = F_{i,j}^{n,n-1}, \\ \dfrac{\omega_{i,j}^{k+1} - \omega_{i,j}^{k+\frac{1}{2}}}{\tau/2} + \omega_{i,j}^{k+1} \\ -\dfrac{\nu\delta t}{2}\left[\dfrac{2}{h_i + h_{i-1}}\left(\dfrac{\omega_{i+1,j}^{k+\frac{1}{2}} - \omega_{i,j}^{k+\frac{1}{2}}}{h_i} - \dfrac{\omega_{i,j}^{k+\frac{1}{2}} - \omega_{i-1,j}^{k+\frac{1}{2}}}{h_{i-1}}\right)\right. \\ \left. + \dfrac{2}{h_j + h_{j-1}}\left(\dfrac{\omega_{i,j+1}^{k+1} - \omega_{i,j}^{k+1}}{h_j} - \dfrac{\omega_{i,j}^{k+1} - \omega_{i,j-1}^{k+1}}{h_{j-1}}\right)\right] \\ = F_{i,j}^{n,n-1}. \end{cases} \tag{7}$$

This implicit numerical scheme can be solved by the method of alternative directions.

Iterations over k with step τ continue until the difference between ω^{k+1} and ω^k is less than some small value ε (in our case we used $\varepsilon = 10^{-8}$). Then, for obtaining new values for stream function ψ, the Poisson equation $\Delta\psi = \omega$ can be solved with known function ω, and new components of velocity field, u and v, can be calculated.

The second-order approximation of boundary conditions for vorticity were used in this case.

Note also that this algorithm is of second-order accuracy both in time and in space.

2.1.2. *Application of Fast Fourier Transform (FFT) for Solution of the Poisson Equation*

The Poisson equation for stream function (4) was solved by the method of separation of variables using FFT with expansion in series along the x-direction (the grid was uniform in that direction) and sweep along the y-direction.

To specify details we write down a sinus Fourier transformation of functions ψ and ω:

$$\psi_{i,j} = \sum_{k=1}^{N_x - 1} a_{k,j} \sin\left(\frac{\pi k i}{N_x}\right);$$

$$\omega_{i,j} = \sum_{k=1}^{N_x - 1} b_{k,j} \sin\left(\frac{\pi k i}{N_x}\right), \tag{8}$$

where $j = 1, \ldots N_y - 1$, and

$$a_{k,j} = \frac{2}{N_x} \sum_{i=1}^{N_x - 1} \psi_{k,j} \sin\left(\frac{\pi k i}{N_x}\right),$$

$$b_{k,j} = \frac{2}{N_x} \sum_{i=1}^{N_x - 1} \omega_{k,j} \sin\left(\frac{\pi k i}{N_x}\right).$$

We discretize the Poisson equation in the following way:

$$\frac{\psi_{i+1,j} - 2\psi_{i,j} + \psi_{i-1,j}}{h_x^2} + \frac{2}{h_{y,j} + h_{y,j-1}} \times \left(\frac{\psi_{i,j+1} - \psi_{i,j}}{h_{y,j}} - \frac{\psi_{i,j} - \psi_{i,j-1}}{h_{y,j-1}}\right) = \omega_{i,j}. \tag{9}$$

This equation can also be written in the form:

$$\psi_{i+1,j} + \psi_{i-1,j} + \alpha_j \psi_{i,j} + \beta_j \psi_{i,j+1} + \gamma_j \psi_{i,j-1} = h_x^2 \omega_{i,j}, \tag{10}$$

where

$$\alpha_j = -2 - h_x^2 (R_j + Q_j),$$
$$\beta_j = h_x^2 R_j, \quad \gamma_j = h_x^2 Q_j,$$
$$R_j = \frac{2}{h_{y,j}(h_{y,j} + h_{y,j-1})},$$
$$Q_j = \frac{2}{h_{y,j-1}(h_{y,j} + h_{y,j-1})}.$$

The substitution of (8) into (10) yields:

$$\sum_{k=1}^{N_x - 1} \left\{ a_{k,j} \left[\sin\frac{\pi k(i+1)}{N_x} + \sin\frac{\pi k(i-1)}{N_x} + \alpha_j \sin\frac{\pi k i}{N_x} \right] + a_{k,j+1}\beta_j \sin\frac{\pi k i}{N_x} + a_{k,j-1}\gamma_j \sin\frac{\pi k i}{N_x} \right\} = h_x^2 \sum_{k=1}^{N_x - 1} b_{k,j} \sin\frac{\pi k i}{N_x}. \tag{11}$$

By comparing the coefficients of the same Fourier harmonics we obtain the following set of equations for $j = 1, \ldots, N_y - 1$:

$$\beta_j a_{k,j+1} + \lambda_{k,j} a_{k,j} + \gamma_j a_{k,j-1} = h_x^2 b_{k,j}, \qquad (12)$$

where $\lambda_{k,j} = \alpha_j + 2\cos(\pi k / N_x)$.

Solution of Eq. (12) by the sweep method gives the coefficients a_k for each j. Then, using (10), we can evaluate a solution for the function $\psi_{i,j}$.

It is well known that the computational speed of the method described increases significantly if the number of nodes is equal to 2^m, where m is an integer. This needs to be taken into consideration in choosing the parameters of the problem.

2.1.3. Parameters

The method described above was applied for the study of both monopole and dipole vortex dynamics. The computations were carried out for the following parameters:

- rectangular domain with the space size 36 along the x- and y-directions (in units of vortex' radius);
- grid size: $N_x = N_y = 257$, 513 and 1025 nodes;
- viscosity coefficients ν: 10^{-4}, $2 \cdot 10^{-4}$, 10^{-3}, $2 \cdot 10^{-3}$, 10^{-2};
- precision parameter ε: 10^{-8}.

2.1.4. Conclusions

The method looks quite appropriate for relatively small viscosity (ν ranges from 10^{-4} to $2 \cdot 10^{-3}$). But for $\nu \sim 10^{-2}$, the numerical scheme was unstable, the energy integral grew with time and some unphysical results appeared. Probably, large viscosity proceeds at sufficiently small time steps, and the numerical scheme can work, nevertheless. But this problem is beyond the scope of our research.

When one employs an implicit method of three-layer solution, one has to store data from the two previous computational time steps, which specifies more stringent requirements to the available computer memory.

2.2. The Second Method

The second numerical scheme is used for *periodical* boundary conditions along the x- and y-directions. For uniformly moving objects, say, dipole vortices, it is convenient to rewrite the basic Eq. (1) in the Gallilean coordinate frame moving along the x-axis with constant velocity U:

$$\frac{\partial \omega}{\partial \tau} - U\frac{\partial \omega}{\partial \xi} + \beta\frac{\partial \psi}{\partial \xi} + J(\psi, \Delta\psi) = \nu\Delta\omega + (\nu a^2 - \gamma)(\omega + a^2\psi), \qquad (13)$$

where $\omega = \Delta\psi - a^2\psi$ and

$$\begin{cases} \xi = x - Ut, \\ \tau = t. \end{cases}$$

In particular cases, when we consider stationary monopole vortices, we put $U = 0$.

2.2.1. Discretization

Central differences both in time and space were used for derivatives within the framework of this scheme; whereas the Laplacian $\Delta\omega$ was calculated by the Duffort-Frankel method, Anderson *et al.* (1984):

$$\Delta\omega \approx \frac{\omega^n_{i+1,j} - \omega^{n-1}_{i,j} - \omega^{n+1}_{i,j} + \omega^n_{i-1,j}}{h_x^2} + \frac{\omega^n_{i,j+1} - \omega^{n-1}_{i,j} - \omega^{n+1}_{i,j} + \omega^n_{i,j-1}}{h_y^2}.$$

Clearly, the unknown value $\omega^{n+1}_{i,j}$ at the $n+1$ time step may be expressed explicitly to give the following explicit numerical scheme[1]

$$\omega^{n+1}_{i,j} = \omega^{n-1}_{i,j} + \frac{2\delta t}{h^2 + 4\nu\delta t}\left[\nu(\omega_{i+1,j} + \omega_{i-1,j} + \omega_{ij+1} + \omega_{ij-1})\right.$$

[1]Equal steps h along the x- and y-directions rather than h_x and h_y are taken for simplicity.

$$+h^2(\nu a^2-\gamma)(\omega_{i,j}+a^2\psi_{i,j})$$
$$-\frac{\beta h}{2}(\psi_{i+1,j}-\psi_{i-1,j})+h^2J(\omega,\psi)\Big]\Big|^n. \quad (14)$$

The problem was solved employing the iteration process of the difference Eq. (14) for each time step. On finding the value of $\omega_{i,j}^{n+1}$ we used it for evaluation of $\psi_{i,j}^{n+1}$ within the framework of Helmholtz equation $\Delta\psi-a^2\psi=\omega$ with known ω.

The Jacobian was calculated as follows: To realize periodic boundary conditions, four different regions are distinguished inside the computational domain:

- The main region includes all mesh points, except the first row and the first column. Vorticity values for these points are obtained from an ordinary difference Eq. (14).
- The second region consists of the points of the first row, and the following index transformation is used: $i-1\to N-1$.
- Analogously, the third region consists of the points of the first column, and the transformation $j-1\to M-1$ is employed.
- The fourth region is simply one point with indexes 1, 1, and the tranformation $i-1\to N-1, j-1\to M-1$ is used.

During the computation cycle the values from the second, third and fourth regions are copied to the last row, last column and right top point, respectively.

2.2.2. *Parameters*

This method was used for both monopole and dipole vortices. The space size was typically 72×72 (measured again in the radius of a vortex), the grid mesh was 513×513 and 1025×1025 points.

The value for the time step was chosen following the Courant-Lewy criterion $\delta t<\delta h/V$, where V is the characteristic velocity of the vortex. Typical values of δt varied in the range 10^{-4} to 10^{-2} depending on the initial conditions.

2.2.3. *Conclusions*

The second method takes less memory resources than the first one. Larger space domains and grid meshes may be used. Hence, a better resolution of a vortex field can be achieved. In addition, the explicit numerical scheme takes a little less CPU time for calculations. However, a more careful choice of the time step δt is required for this scheme.

3. DYNAMICS OF MONOPOLE VORTICES

For axisymmetric monopole vortices in an uniformly rotating ($\beta=0$) unbounded fluid, the basic Eq. (1) reduces to a linear one (the Jacobian is equal to zero identically for axisymmetric motion):

$$\frac{\partial}{\partial t}(\Delta\psi-a^2\psi)=\nu\Delta^2\psi-\gamma\Delta\psi. \quad (15)$$

We can formally construct an "exact" analytical solution of this equation with the aid of separation of variables:

$$\psi(r,t)=e^{-\alpha t}\begin{cases}A_1J_0(\eta r)+A_2I_0(\mu r), & r<r_0;\\ A_3K_0(\mu r), & r>r_0.\end{cases} \quad (16)$$

Here and below, $J_i(x)$ are the Bessel functions of order i, $I_i(x)$ and $K_i(x)$ are the modified Bessel functions of order i,

$$A_2=\frac{A_1}{\mu}\frac{\eta J_1(\eta r_0)K_0(\mu r_0)-\mu J_0(\eta r_0)K_1(\mu r_0)}{I_1(\mu r_0)K_0(\mu r_0)+I_0(\mu r_0)K_1(\mu r_0)},$$
$$A_3=\frac{A_1J_0(\eta r_0)+A_2I_0(\mu r_0)}{K_0(\mu r_0)},$$
$$\mu_i^2=\frac{a^2}{\nu}\frac{\gamma+\nu\eta_i^2}{a^2+\eta_i^2},$$

η_i is one of the roots of the Bessel function $J_0(\eta_i r_0)=0$, and r_0 is the radius of the vortex core. The vortex damping rate is

$$\alpha_i=\eta_i^2\frac{\gamma+\nu\eta_i^2}{a^2+\eta_i^2}. \quad (17)$$

The solution has a smooth profile up to the second-order derivative with respect to r, so that the velocity and vorticity fields are both continuous. But the third- and higher-order derivatives of the function ψ have discontinuity at the vortex boundary at $r = r_0$.

This solution is quite appropriate for semiviscous models of vortex motion, when the viscosity occurs, mainly, inside the vortex core and is negligible in the outer region. But in an uniformly viscous fluid, the vorticity diffusion proceeds from the vortex core outwards. This diffusion is important only when $\nu \neq 0$, *i.e.*, when the internal Reynolds viscosity is taken into account. When the external viscosity dominates ($\nu \to 0$), one can neglect the diffusion process at the vortex-core border and consider the solution above to be exact.

In this section we investigate numerically the behaviour of the monopole vortices described by the formula (16) at the initial instant of time under the action of different factors, such as internal and external viscosity and homogeneous fluid rotation.

3.1. The Influence of Internal Viscosity on the Evolution of Monopole Vortices

Consider first the case of nonrotating fluid ($a = \beta = 0$) and neglect external viscosity $\gamma = 0$. Then, the solution (16) readily reduces to

$$\psi(r, t) = A e^{-\alpha t} \begin{cases} J_0(\eta r), & r < r_0; \\ -\eta r_0 J_1(\eta r_0) \ln \frac{r}{r_0}, & r > r_0, \end{cases} \quad (18)$$

where $\alpha = \nu \eta^2$.

The vorticity field can be written as

$$\omega(r, t) = -A \eta^2 e^{-\alpha t} \begin{cases} J_0(\eta r), & r < r_0; \\ 0, & r > r_0. \end{cases} \quad (19)$$

This means that the fluid motion is potential outside the vortex core ($r > r_0$). Although the vorticity field is continuous, it has a singularity (discontinuity of the 1-st kind) in the derivative at the vortex boundary $r = r_0$ (see Fig. 1 for $t = 0$).

This singularity is very important because in evaluation of the right-hand side of Eq. (15) it is necessary to evaluate the derivatives of ω up to the second-order of magnitude ($\Delta^2 \psi \equiv \Delta \omega$). The finite spatial step of the numerical scheme leads to a smoothed vorticity profile (see the corresponding curves in Fig. 1 for $t \neq 0$) and, consequently, to diffusion of vorticity. Eventually, the monopole vortex changes its shape and transforms into a different axisymmetric monopole structure without any singularities either in the profile or in its derivatives. Apparently, we can interpret such a transition as structural instability of the analytical solution (15).

The theoretical dependences of vortex intensity $\omega_{\max}$ and energy $E = \iint [(\nabla \psi)^2 + a^2 \psi^2] \, d\vec{r}$ on time (dashed curves) and the dependences calculated by the first numerical method (solid curves) are compared in Figure 2. One can see a pronounced discrepancy between the analytical solution (18) for singular vortex decay and for a smooth numerical solution. The latter decays slowly in time and, obviously, not exponentially (exponential decay corresponds to straight lines at the semilogarithmic scale in the plot).

Another reason for this discrepancy is finiteness of the numerical domain. So that, instead of the solution (18), (19) for the unbounded domain, we have a truncated part of this solution as an initial perturbation. Note that the outer part of the function ψ does not decay with distance, it growths instead.

So, we can conclude that in the course of evolution, the initial perturbation transforms into some new monopole vortex with a smooth profile that is more stable with respect to the influence of Reynolds viscosity than the vortices having singularities either in the vorticity profile or in its derivatives.

3.2. The Influence of External Viscosity on the Evolution of Monopole Vortices

The external viscosity is described by the term proportional to γ in Eq. (15). This case with $a = \beta = \nu = 0$ is trivial for analytical solution that

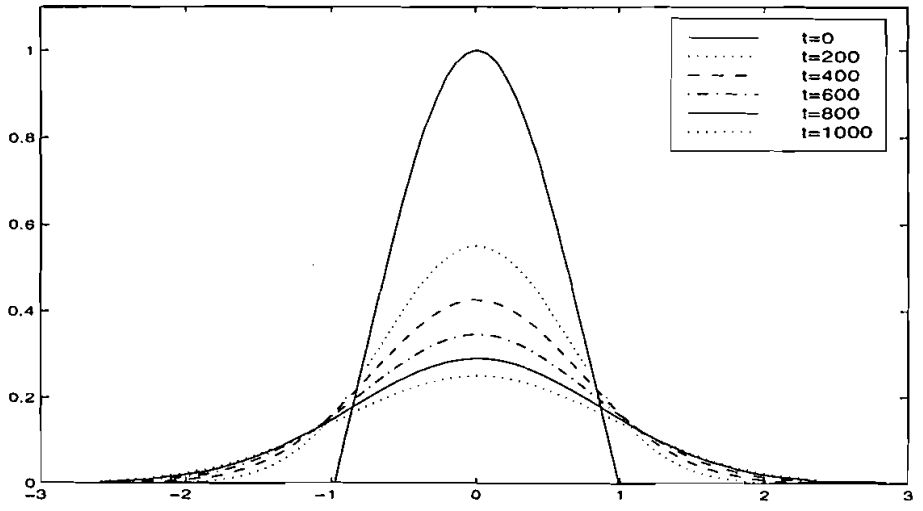

FIGURE 1 Vorticity profile *versus* radius for the simplest monopole vortex at different instants of time ($\nu = 2 \cdot 10^{-3}$, $\gamma = 0$).

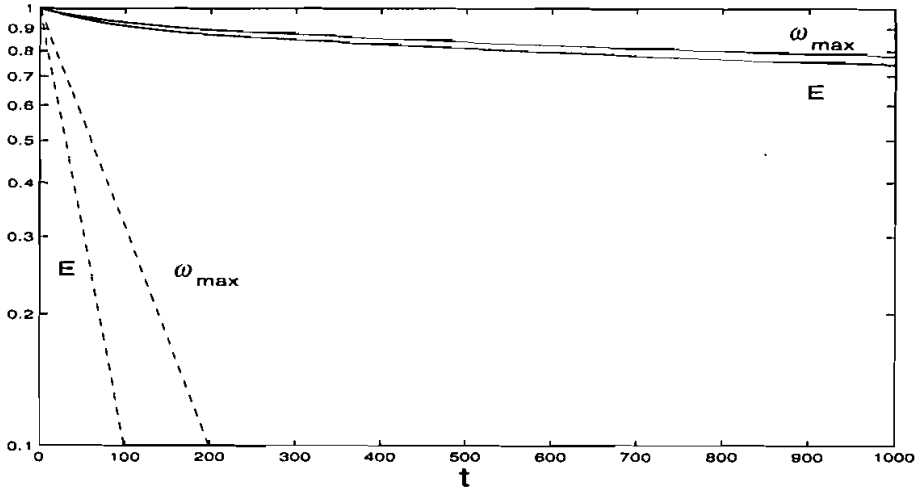

FIGURE 2 Theoretical time dependences of monopole vortex amplitude ω_{max} and energy E (dashed curves) and analogous dependences obtained numerically (solid curves) at a semilogarithmic scale ($\nu = 2 \cdot 10^{-3}$, $\gamma = 0$). Time is measured in the period of vortex rotation.

can be represented in the same form as (18) but with $\alpha = \gamma$.

Using the second numerical method we carried out a set of experiments with γ ranging from $2 \cdot 10^{-4}$ to $2 \cdot 10^{-3}$. We obtained, again, some disagreements between theory and numerical results (see Fig. 3) which are caused, in our opinion, by the finite size of the numerical domain.

Note that in this case there is no vorticity diffusion from the vortex core outwards.

3.3. The Influence of Rotation on the Dynamics of Monopole Vortices

In this subsection we study only the influence of uniform rotation on vortex decay, *i.e.*, the

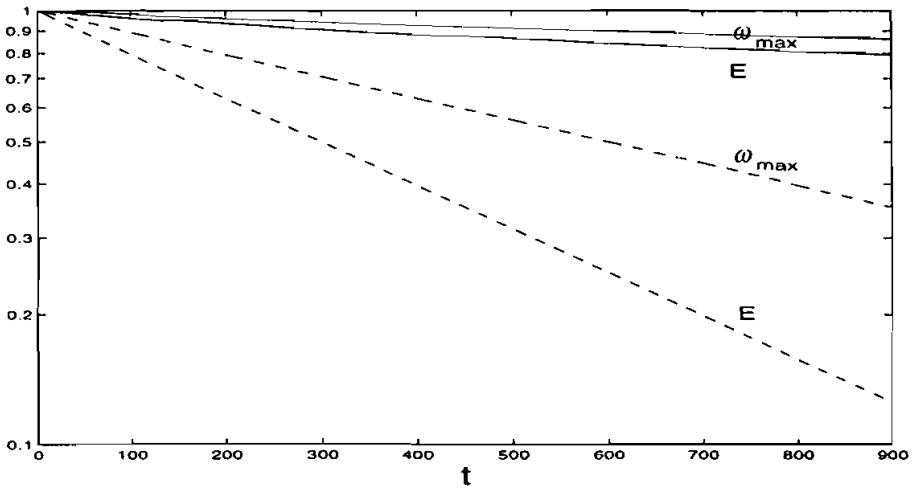

FIGURE 3 Theoretical dependences of monopole vortex amplitude ω_{max} and energy E on time (dashed curves) and analogous dependences obtained numerically (solid curves) at a semilogarithmic scale ($\nu = 0$, $\gamma = 2 \cdot 10^{-3}$).

influence of the parameter a in Eq. (15). We will omit from consideration the β-effect upon vortex evolution and decay. (The β-effect on the dynamics of monopole vortices in an inviscid fluid was studied in Reznik and Dewar (1994); Sutyrin *et al.* (1997), see also the literature cited therein.)

According to the analytical solutions (16), (17), the vortex damping rate decreases with increasing rotation parameter a. We checked this theoretical prediction in numerical experiments employing the second numerical method separately for internal and external viscosities.

Inasmuch as the analytical solution (16) is unstable in a fluid with internal viscosity ($\nu \neq 0$, $\gamma = 0$) and transforms into another one with a completely smooth profile and bearing in mind the influence of the finite domain size, it is not surprizing that the numerical results obtained differ from the theoretical ones. Actually, we revealed that the vortex decay dependence on a is not monotonic. The vortex damping rate first decreases, as a grows, but then it increases again. In Figure 4 one can see the dependence of energy and enstrophy, $S = 1/2 \iint \omega^2 d\vec{r}$, on time for different values of a.

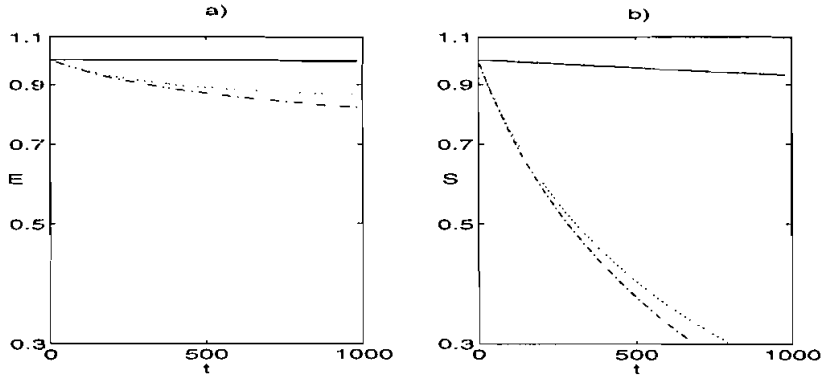

FIGURE 4 Dependences of energy (a) and enstrophy (b) on time for different values of rotation parameter a: solid curve – $a^2 = 0.01$; dotted-dashed curve – $a^2 = 0.25$; dotted curve – $a^2 = 0.6$ ($\nu = 2 \cdot 10^{-4}$ in all cases.)

Qualitatively the same behaviour of energy and enstrophy on a was obtained for the case of external viscosity.

4. DYNAMICS OF SINGLE DIPOLE VORTICES

The dipole vortices have a more complex structure and behaviour than the monopole ones. As we have mentioned above, exact solutions in the form of dipole vortices (ChL vortices) are known for a two-dimensional case of inviscid fluid. They have continuous profiles both for the stream function ψ and for the vorticity field ω and singularities in vorticity derivatives. An interesting feature of such vortices is that the vorticity is concentrated only inside their cores and is equal to zero outside, so that the fluid motion in the outside domain is potential. The stream function decays relatively weakly in the outside domain as an inverse power of distance, $\psi \sim r^{-1}$, although the velocity field decays more rapidly, $|\mathbf{v}| \sim r^{-2}$.

Similar vortices may exist in a plane and on a rotating sphere in a shallow rotating fluid, Stern (1975); Larichev *et al.* (1976); Tribbia (1984); Verkly (1984), but they decay faster at the infinity, as $e^{-\mu r}/\sqrt{r}$. We do not know any generalizations of such solutions for viscous fluid.

4.1. Analytical Solution for Dipole Vortices in Viscous Fluid

One simple case can be considered analytically if we assume that the fluid trapped inside the vortex core is viscous and the surrounding fluid is ideal. Such an assumption can be proved speculatively by the circumstance that the fluid involved in the rapid motion inside the vortex core of radius r_0 possesses turbulent viscosity rather than the laminar one in the surrounding fluid. Therefore, we will seek for a solution for nonrotating fluid ($a = \beta = 0$) with a potential flow outside the vortex core. The vortex will decay due to the presence of inside viscosity, and its intensity and velocity will decrease gradually in time.

Let us make a transformation:

$$\xi = x - \int_0^t V(t')\,dt', \quad y = y, \quad t = t.$$

Then, the basic equation takes a form:

$$\frac{\partial}{\partial t}\Delta\psi + J(\psi + V(t)y, \Delta\psi) = \nu\Delta^2\psi - \gamma\Delta\psi. \quad (20)$$

We will seek a solution having the spatial structure like that of the ChL vortex but with variable parameters. The Jacobian in (20) is equal to zero for such vortices, and the remaining part of the equation for vorticity, $\omega = \Delta\psi$, is nothing but an ordinary linear duffusion equation. In other words, we try to find a solution that would satisfy the system

$$\begin{cases} J[\psi + V(t)y, \Delta\psi] = 0, \\ \frac{\partial\omega}{\partial t} = \nu\Delta\omega - \gamma\omega. \end{cases} \quad (21)$$

The solution of the first equation of the set (21) can be represented in a polar coordinate system:

$$\psi(r, \varphi, t) = -\frac{2V(t)}{J_2(\zeta_i)}\sin\varphi \times \begin{cases} \frac{J_1[\eta_i(t)r]}{\eta} + \frac{J_2(\zeta_i)}{2}r, & r \le r_0(t); \\ \frac{r_0^2(t)J_2(\zeta_i)}{2r}, & r > r_0(t), \end{cases} \quad (22)$$

where $\zeta_i \equiv \eta_i r_0$ is the i-th root of the Bessel function $J_1(z)$.

Substituting this solution into the second equation of the set (21) we find that it satisfies this equation if neither r_0 nor η depend on t, but the vortex velocity (and its intensity) depend on time as $V(t) = V_0 e^{-(\nu\eta^2+\gamma)t}$.

For this solution the vorticity is a continuous function of spatial coordinates. It is equal to zero at the boundary of the vortex core and conserves this value in the outside region where the fluid motion is potential. Higher-order derivatives of

vorticity, however, have singularities at the point $r = r_0$, which leads to vorticity diffusion in real fluids. Note that in the case $\nu = 0$ but $\gamma \neq 0$, there is no vorticity diffusion and the solution (22) remains valid for all times.

4.2. Dipole Vortex Decay and Interaction with the Wall in Nonrotating Viscous Fluid

It was assumed that the fluid has the same uniform viscosity in the entire domain, and the initial condition in the form of the ChL vortex (22) was first set for the first root of the Bessel function $J_1(\zeta_1)$, $\zeta_1 = 3.8317$. We observed a sort of vortex adaptation to the viscous surrounding at the initial stage of its motion. Some secondary small vortices were generated behind the major one. Vortices-satellites had significantly lower amplitudes but were quite stable and formed a turbulent tail which was pronounced throughout the calculation time. This process of secondary vortex generation behind the major vortex is illustrated in Figure 5.

When the vortex propagates far from the walls, it demonstrates a behaviour which is very close to the theoretical prediction, *i.e.*, it decreases gradually and conserves its shape. In Figure 6 one can see comparison of theoretical and numerical results for the adiabatic vortex decay in viscous fluid. But its behaviour becomes rather complex near the wall. That is why there is a certain discrepancy between numerical and theoretical results in Figure 6 for $t \geq 60$.

An interesting rebound phenomenon is observed near the wall. This phenomenon was discovered recently in the paper by Carnevale, Velasco . Fuentes, Orlandi (1997). It is well-known that a rigid wall plays a role of ideal mirror for vortices in a perfect fluid (see, *e.g.*, Batchelor (1970)). It means that the interaction of a vortex with a wall can be considered as a head-on collision of two vortices of the same intensity moving in opposite directions: the vortices reconnect on collision, and two new vortices moving in the direction perpendicular to the initial one arise. In other words, near the wall, a dipole vortex splits into two monopole vortices moving in opposite directions along the wall.

The situation may be quite different in a viscous fluid due to the presence of a viscous boundary layer near the wall. Vortex rebound depends on the relationship between its intensity and fluid viscosity. One of the examples of vortex rebound from a nonslip wall is illustrated in Figure 7.

One can see in Figure 7 that the vortex approaching the wall deforms the viscous boundary layer and breaks away from it some small vortices which are trapped by the major vortex. Meanwhile, the major vortex splits into two parts moving in opposite directions along the arc-type trajectory away from the wall. Then, new pairs of

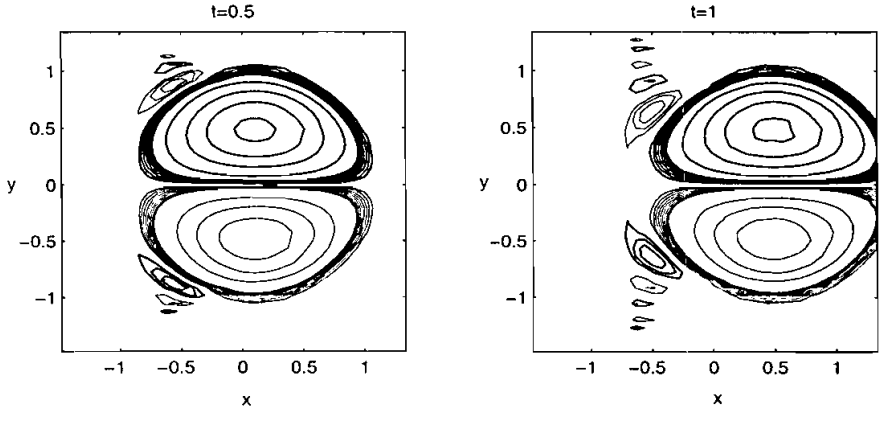

FIGURE 5 Generation of secondary vortices in the course of propagation of the major dipole vortex for $\nu = 10^{-4}$, $\gamma = 0$.

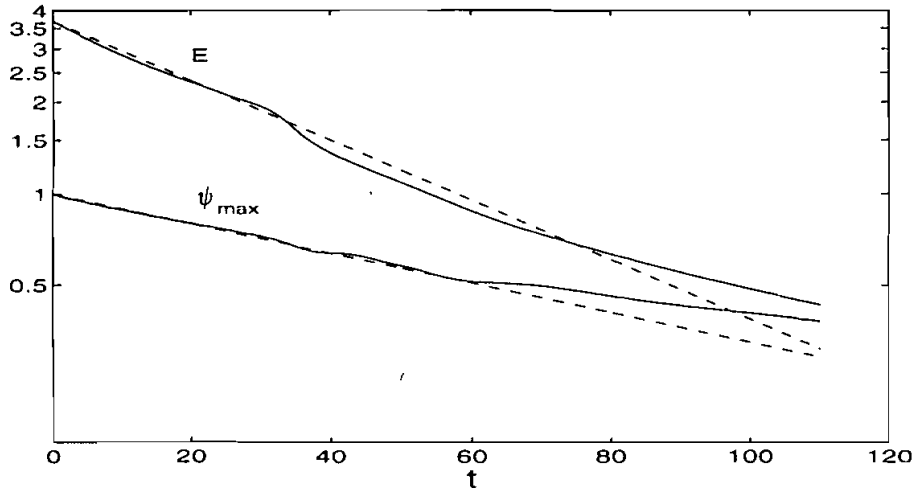

FIGURE 6 Energy E and maximum of stream function ψ_{max} dependences on time for dipole vortex in viscous fluid ($\nu = 2 \cdot 10^{-3}$, $\gamma = 0$).

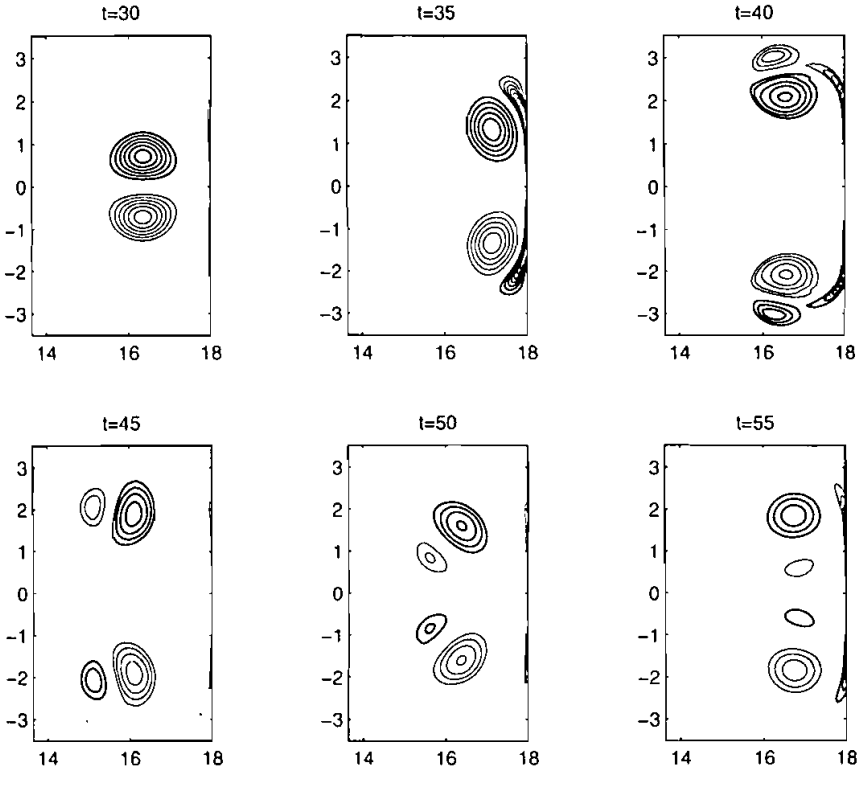

FIGURE 7 Interaction of dipole vortex with a wall in viscous fluid ($\nu = 2 \cdot 10^{-3}$, $\gamma = 0$).

vortices having different intensities approach the wall again and interact with it and with each other. But after the second rebound the vortex intensity decreases and they no longer have a strength to come to the wall again. They gradually stop at some distance from the wall and, eventually, dis-

appear completely. The trajectories of the maximum and minimum of the major vortex are depicted in Figure 8a.

As was mentioned in Carnevale *et al.* (1997), such a complex rebound occurs only in a very small range of initial vortex velocities V_0. In our calculations this phenomenon was observed for $V_0 = 0.7692$ at $\nu = 2 \cdot 10^{-3}$, $\gamma = 0$, while only simple rebound without any loops was observed for $V_0 = 1.0$ and the same viscosities (see Fig. 8b).

The same vortex demonstrates a different behaviour near the wall in the case of very small internal viscosity, $\nu = 10^{-4}$. Its collision with the wall is similar to that in a perfect fluid at the initial stage: it splits into two monopole vortices moving along the wall in opposite directions. Nevertheless, it strongly interacts with a boundary layer, breaks away some vortices from it and interacts with them. This process is illustrated in Figure 9 for the left monopole of the initial vortex.

This strong interaction of the vortex with the boundary layer leads to a more pronounced decay than in the case of head-on collision of two dipole vortices (see below) in the absence of a boundary layer. Two vortex satellites are gradually formed from the boundary layer, and the tripole vortex ensemble moves away from the wall rotating around their common center and decaying smoothly. Trajectories of the maximum and minimum of initial dipole vortex are depicted in Figure 8c. It is interesting to note that the initial intensity of the satellites is larger than the intensity of the monopole vortex, but they have smaller sizes and decay faster, so that only the monopole structures are distinguishable on both sides of the initial direction of vortex motion at the final stage of decay.

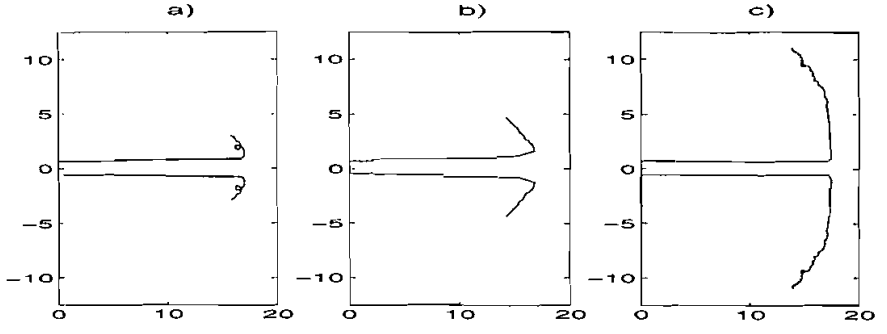

FIGURE 8 Trajectories of the vortex maximum and minimum near the rigid wall. (a) – complex rebound with the loops at initial vortex velocity $V_0 = 0.7692$ ($\nu = 2 \cdot 10^{-3}$, $\gamma = 0$); (b) – simple rebound without loops at $V_0 = 1.0$ and the same viscosities; (c) – simple rebound in the fluid of small viscosity $\nu = 10^{-4}$, $\gamma = 0$ at $V_0 = 0.7692$.

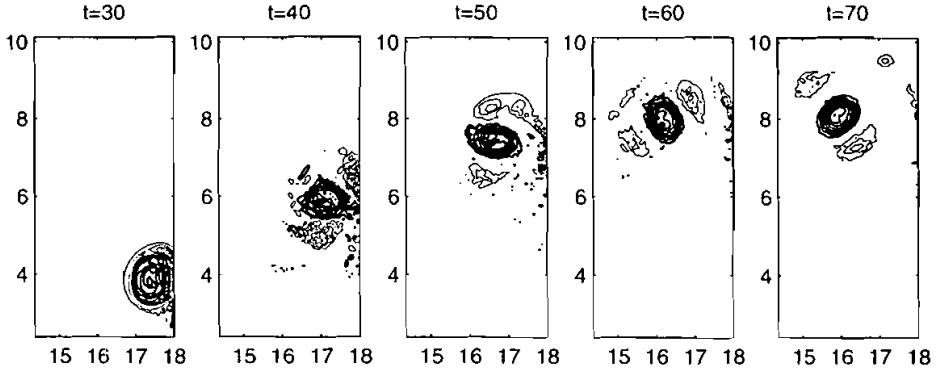

FIGURE 9 Vorticity contours for the left half of the dipole vortex near the wall ($\nu = 10^{-4}$).

So, we see that the interaction of a vortex with a rigid wall in a viscous fluid is an interesting and topical problem. We discovered some characteristic features of the interaction and described some of the features considered earlier in Carnevale *et al.* (1997). The results described are incomplete, in our opinion, and need more detailed investigation in the future.

5. INTERACTIONS OF DIPOLE VORTICES

The process of vortex interaction in a viscous fluid is pretty interesting and has some specific features. We shall consider it here only for the ChL vortices.

5.1. Overtaking Interaction of the Chaplygin-Lamb Vortices

We consider first the interaction of two vortices moving in the same direction along the x-axis. Such vortices demonstrate soliton-like behaviour in an ideal fluid or in a fluid of very small viscosity. They survive on collision with approximately the same parameters. This was confirmed numerically (Fig. 10a) for the case of small viscosity ($\nu = 10^{-6} - 2 \cdot 10^{-4}$, $\gamma = 0$).

However, in a more viscous case ($\nu = 10^{-3}$, $\gamma = 0$) we revealed complete destruction of the first small vortex on interaction with the larger one. It is illustrated in Figure 10b.

Perhaps, the character of vortex interaction depends not only on the value of viscosity but also on the ratio of their velocities and, maybe, for some ratios of velocities, quasi-soliton interaction between vortices takes place in a wide range of viscosity parameter, but we have not studied this problem in detail.

5.2. Head-on Collision of the Chaplygin-Lamb Vortices

We studied numerically the head-on collision of two ChL vortices of the same intensities and sizes

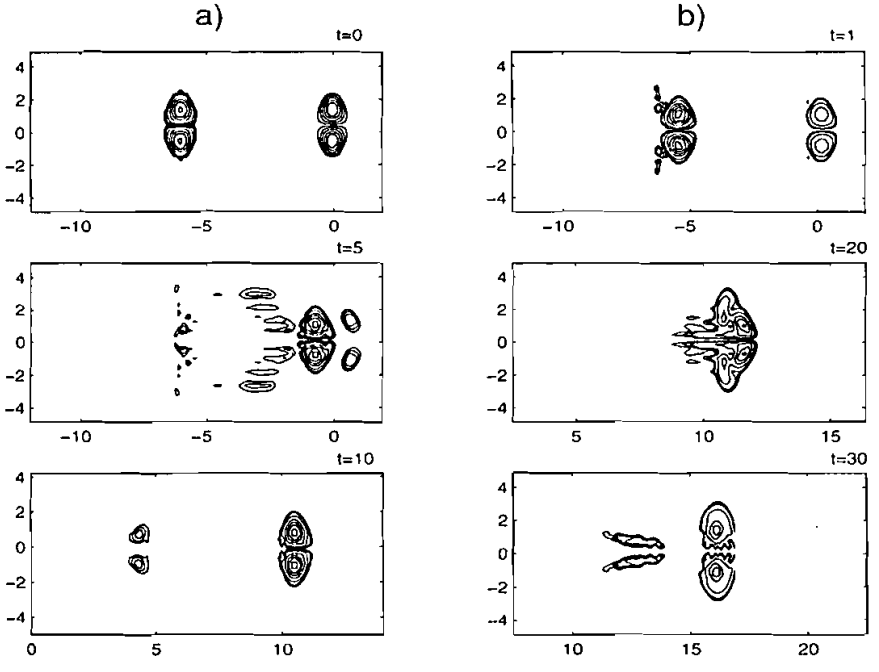

FIGURE 10 Overtaking interaction of two ChL vortices: (a) – in a fluid of small internal viscosity ($\nu = 2 \cdot 10^{-4}$, $\gamma = 0$); (b) – in a more viscous fluid ($\nu = 10^{-3}$, $\gamma = 0$).

moving in opposite directions along the x-axis. Before collision, the vortices moved in a usual manner described above, decaying gradually in time. The process of collision was very similar to the vortex interaction in inviscid fluid or to the vortex rebound from the wall in an inviscid fluid: each vortex split into two parts which reconnected with their counterparts and began to move in opposite directions along the y-axis. This picture is illustrated in Figures 11a, b for the time interval from 0 to 140 approximately.

When the vortices approached the walls we observed a usual vortex behaviour for the viscous case described above. Much stronger dissipation took place for the vortices near the wall. So, in contrast to the inviscid case, the vortex head-on collision with each other and their interaction with a rigid wall are different due to the influence of the viscous boundary layer near the wall in the latter case.

5.3. Head-on Collision of the Chaplygin-Lamb Vortices with Shifted Centers

We studied an interesting case of head-on collision with shifted centers of two ChL vortices of the same intensity. In the course of interaction, two dipole vortices merged into one complex structure which then split again into two pairs of dipole vortices moving at an angle of $\pi/4$ to the initial trajectories, and to some shapeless vortex field between them (Fig. 12). The interaction was inelastic, some residual small-scale vortices were produced and remained in the region of collision, but two well-formed dipole vortices left this region.

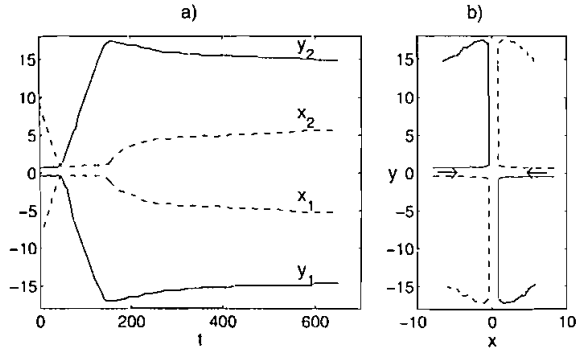

FIGURE 11 Dependences of the ChL dipole maximum and minimum on time (a) and their trajectories in the x, y-plane (b). Initial velocities of the vortices $V_0 = \pm 0.1$, $\nu = 2 \cdot 10^{-4}$, $\gamma = 0$.

5.4. Dynamics and Stability of Dipole Vortices with Complex Internal Structure

In the research described above we used initial conditions for both ChL and LR vortices with the first roots of the corresponding "eigenvalue equations" for η_i. If we choose the second, or higher-order roots, then new dipole vortices appear with a more complex structure of the vortex cores (the outer structure of vortices is unchanged and, in the case of the ChL vortex, coincides with the potential flow around a cylinder). Stability of such vortex structures was not studied yet and we examine this problem for ChL vortices for a fluid with internal viscosity.

So, we consider the analytical solution (22) of Eq. (20) with $\gamma = 0$ for the second root of the Bessel function $J_1(\zeta_2)$, $\zeta_2 = 7.0156$. We note that, for the same value of r_0, the larger the order of the root (the larger the value of η_i), the more pronounced the vortex decay in time ($V(t) \sim e^{-\nu\eta_i^2 t}$). The initial vortex structure is shown in Figure 13.

A dipole-type vortex surrounded by a pair of bended, elliptically shaped monopole vortices of opposite polarities is distinct inside the vortex core of radius r_0. Theoretically, this vortex pattern must move stationarily along the x-axis. But numerical experiment shows that this configuration is unstable and has complex behaviour due to small perturbations (finiteness of the numerical domain, errors of truncations, *etc.*) The outside pair of vortices begins to oscillate with respect to the inside dipole which also does not remain stationary but pulsates instead (Fig. 14). Eventually, the initial vortex structure is destroyed, and new dipole vortices and vortex pairs appear. At the same time, these secondary vortices interact with

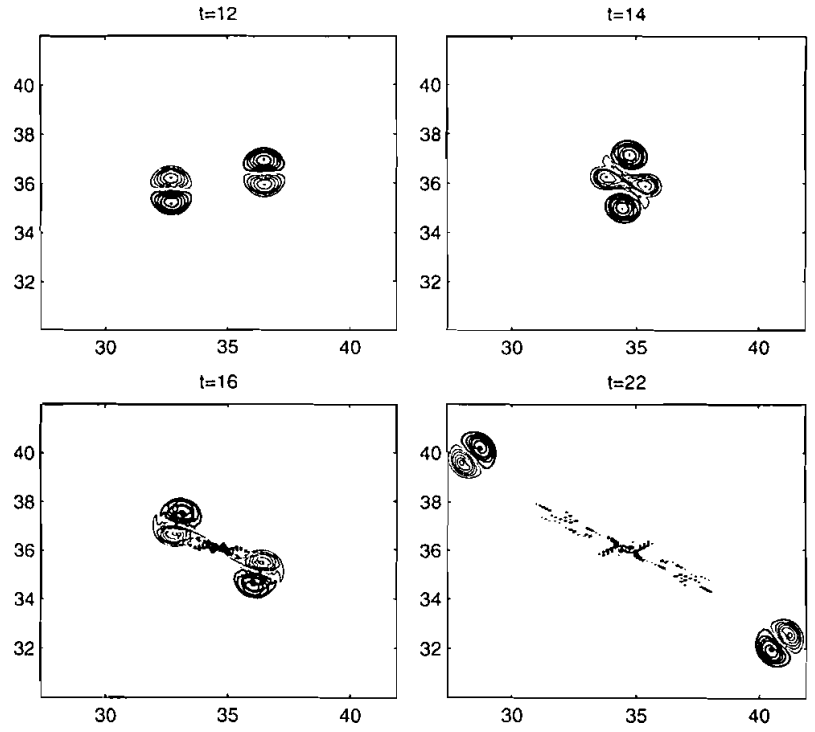

FIGURE 12 Vorticity contours for ChL dipole interaction with shifted centers.

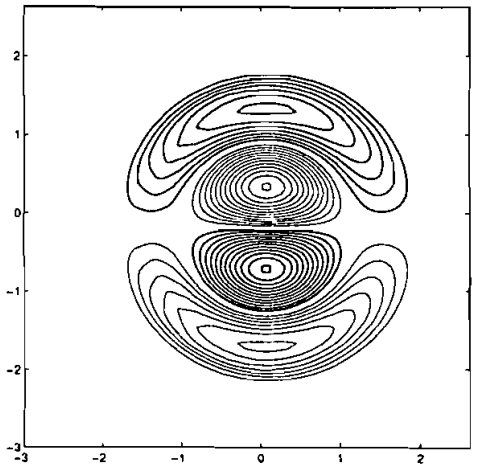

FIGURE 13 Vorticity line levels of the dipole ChL vortex with complex internal structure of radius $r_0 = 2$ and $\eta_2\, r_0 = 7.0156$.

each other and with some residual small-amplitude vortices so that their dynamics looks rather complex. These calculations also support the idea that the dipole vortices are rather robust and can be formed under arbitrary (in some sense) initial conditions.

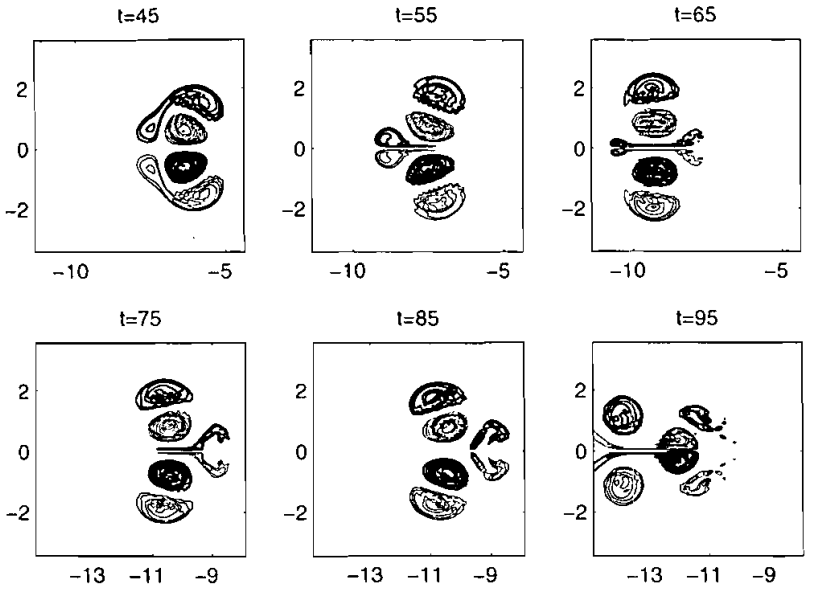

FIGURE 14 Dynamics of ChL dipole vortex with a complex internal structure in a viscous fluid ($\nu = 2 \cdot 10^{-4}$, $\gamma = 0$).

6. CONCLUSIONS

We have studied numerically some important features of vortex dynamics in viscous fluid. We have evaluated two-dimensional monopole vortices and discovered that the vortices with any singularities in their profiles are structurally unstable. They transform into monopole vortices of other types with smooth profiles without singularities. The latters decay gradually in time slower than exponentially. Such vortices can exist for a long time in real fluids, especially in geophysical systems (seas, oceans, atmosphere) where the influence of viscosity is not so strong. Fluid rotation (Earth' rotation in geophysics) does not destroy the vortices, but it reduces their damping rate.

Dipole vortices of simple internal structure are more robust with respect to preserving their shape. The main reason for this is that they move in space and escape the region with small amplitude perturbations generated by them in the course of adaptation from the initial parameters to the current ones, while monopole vortices co-exist with such perturbations in the same domain and interact with them for a long time. An analogous effect was described in Gorshkov *et al.* (1996) in the analytical study of vortex evolution under the action of different perturbations. Dipole vortices with complex internal structure are unstable and, in the course of a rather complicated evolution, they break down to form several dipole vortices and vortex pairs as well as some vague vorticity patterns.

We also studied some elementary acts of vortex interactions in viscous fluid both with each other and with rigid walls. An important conclusion follows from this study: Vortex interaction in a fluid of small viscosity can be very similar to the soliton type interaction, *i.e.*, the interacting vortices are not destroyed completely; instead, they survive on collision with approximately the same parameters as they had before. However, they can exchange vortices and change their direction of propagation. But, strictly speaking, dipole vortices are not solitons and, probably, they are destroyed at some angles of collision and lose their individuality. This process has not yet been studied in detail, even for an inviscid fluid. Knowledge of

elementary acts of vortex interactions in viscous fluid is helpful in understanding a general picture of fluid dynamics and especially for explanation of its turbulent properties. We hope that this paper sheds light on these problems.

Acknowledgements

E. A. Babkin and Yu. A. Stepanyants are grateful to all personal staff of the laboratory LSEET, Université de Toulon et du Var for their kind support and benevolent attitude. Special thanks are to Gilles Rougier and Yves Ruin for their useful advice and help with computer-related topics. They are also thankful to A. D. Osipenko for his assistance in the analytical part of the paper and useful discussions, and to N. B. Krivatkina for her help in preparing the manuscript.

This work became possible thanks to the financial support of the program Reseau Formation Recherche "Polynomes Orthogonaux", France, in which E. A. Babkin was involved and thanks to the PAST triennal invited position at the Université de Toulon et du Var for Yu. A. Stepanyants. Besides, the work was also partially supported by INTAS (grant No. 94-4057), RFBR (grants No. 96-05-64476 and No. 96-01-00585), the Project EC MAS3-CT95-0037-FANS, the French Programme National d'Oceanographie Cotiere, and the grants of the Ministry of General and Professional Education of Russia.

References

Agullo, O. and Verga, A. D. (1997) Exact two vortices solution of the Navier-Stokes equations, *Phys. Rev. Lett.*, **78**(12), 2361–2364.

Anderson, D. A., Tannehill, J. C. and Pletcher, R. H. (1984) Computational Fluid Mechanics and Heat Transfer, V. 1, 2, Hemisphere Publishing Corporation, New York.

Batchelor, J. K. (1970) An Introduction to Fluid Dynamics, Cambridge, Cambridge University Press.

Berezovsky, A. and Kaplansky, F. (1992) Dynamics of thin vortex in a viscous fluid, *Proc. Estonian Acad. Sci. Phys. Math.*, **41**(2), 95–103.

Carnevale, G. F., Velasco Fuentes, O. U. and Orlandi, P. (1997) Inviscid dipole-vortex rebound from a wall or coast, *J. Fluid Mech.*, **351**, 75–103.

Dolzhansky, F. V., Krymov, V. A. and Manin, D. Yu. (1990) Stability and vortex structures of quasi-two-dimensional shear flows, *Uspekhi. Fiz. Nauk*, **160**(7), 1–47 (in Russian). See also the English translation In: *Sov. Phys. Uspekhi.*

Flierl, G. R., Larichev, V. D., McWilliams, J. C. and Reznik, G. M. (1980) The dynamics of baroclinic and barotropic solitary eddies, *Dyn. Atmos. Oceans*, **5**, 1–41.

Gorshkov, K. A., Ostrovsky, L. A. and Soustova, I. A. (1996) Perturbation theory for vortices, Preprint IAP RAS, (406), Nizhny Novgorod (in Russian); Gorshkov, K. A., Ostrovsky, L. A. and Soustova, I. A. (1999) Perturbation theory for vortex dynamics, *J. Fluid Mech.*, to be published.

Kamenkovich, V. M., Koshlyakov, M. N. and Monin, A. S. (1988) *Synoptic Vortices in the Ocean*, Gidrometeoizdat, Leningrad, (in Russian).

Kochin, N. E., Kibel', I. A. and Rose, N. V. (1963) Theoretical Hydrodynamics, V. 1, 2, Fizmatgiz, Moscow, (in Russian).

Lamb, H. (1932) Hydrodynamics, 6-th edn., Cambridge University Press, London and New York.

Larichev, V. D. and Reznik, G. M. (1976) On two-dimensional solitary Rossby waves, *Sov. Phys. Doklady*, **231**(5), 1077–1079 (English translation of the Russian journal *DAN SSSR*). See also: Larichev, V. D. and Reznik, G. M. (1976) Two-dimensional Rossby soliton: an exact solution, *Polymode News*, **19**(3), 1–6.

Lavrent'ev, M. A. and Shabat, B. V. (1977) Problems of Hydrodynamics and their Mathematical Models, Nauka, Moscow, (in Russian).

Meleshko, V. V. and Van Heijst, G. J. F. (1994) Interacting two-dimensional vortex structures: point vortices, contour kinematics and stirring properties, *Chaos, Solitons and Fractals*, **4**(6), 977–1010.

Nezlin, M. V. and Snezhkin, E. N. (1993) Rossby Vortices, Spiral Structures, *Solitons*, Springer-Verlag.

Pedlosky, J. (1987) Geophysical Fluid Dynamics, 2-nd edn., Springer-Verlag, New York.

Petviashvili, V. and Pokhotelov, O. (1992) Solitary Waves in Plasmas and in the Atmosphere, Gordon and Breach, Philadelphia.

Reznik, G. M. and Dewar, W. K. (1994) An analytical theory of distributed axisymmetric barotropic vortices on the beta-plane, *J. Fluid Mech.*, **269**, 301–307.

Saffman, P. G. (1992) Vortex Dynamics, Cambridge University Press, Cambridge.

Samarsky, A. A. (1977) The Theory of Difference Schemes, Nauka, Moscow, (in Russian).

Stepanyants, Yu. A. and Fabrikant, A. L. (1992) Features of the "Cherenkov" emission of drift waves in hydrodynamics and in a plasma, *Sov. Phys. JETP*, **75**(5), 818–824 (English translation of the Russian journal *ZhETF*).

Stern, M. E. (1975) Minimal properties of planetary eddies, *J. Marine Res.*, **33**(1), 1–13.

Sutyrin, G. G. and Morel, I. (1997) Intense vortex motion in a stratified fluid on the beta-plane: analytical theory and its validation, *J. Fluid Mech.*, **336**, 203–209.

Tribbia, J. J. (1984) Modons in spherical geometry, *Geophys. Astrophys. Fluid Dyn.*, **30**(1–2), 131–168.

Verkly, W. T. M. (1984) The construction of barotropic modons on a sphere, *J. Atmos. Sci.*, **41**(16), 2492–2504.